Journal of Mathematics in Industry
a SpringerOpen Journal

RESEARCH Open Access

Assessment of self-adapting local projection-based solvers for laminar and turbulent industrial flows

Tomás Chacón Rebollo[1,2], Enrique Delgado Ávila[1,2*], Macarena Gómez Mármol[1] and Samuele Rubino[1,2]

*Correspondence: edelgado1@us.es
[1]Dpto. de Ecuaciones Diferenciales y Análisis Numérico, Facultad de Matemáticas, Universidad de Sevilla, Sevilla, Spain
[2]IMUS, Universidad de Sevilla, Sevilla, Spain

Abstract

In this work, we study the performance of some local projection-based solvers in the Large Eddy Simulation (LES) of laminar and turbulent flows governed by the incompressible Navier–Stokes Equations (NSE). On one side, we focus on a high-order term-by-term stabilization Finite Element (FE) method that has one level, in the sense that it is defined on a single mesh, and in which the projection-stabilized structure of standard Local Projection Stabilization (LPS) methods is replaced by an interpolation-stabilized structure. The interest of LPS methods is that they ensure a self-adapting high accuracy in laminar regions of turbulent flows, which turns to be of overall optimal high accuracy if the flow is fully laminar. On the other side, we propose a new Reduced Basis (RB) Variational Multi-Scale (VMS)-Smargorinsky turbulence model, based upon an empirical interpolation of the sub-grid eddy viscosity term. This method yields dramatical improvements of the computing time for benchmark flows. An overview about known results from the numerical analysis of the proposed methods is given, by highlighting the used mathematical tools. In the numerical study, we have considered two well known problems with applications in industry: the (3D) turbulent flow in a channel and the (2D/3D) recirculating flow in a lid-driven cavity.

Keywords: Large eddy simulation; Local projection simulation; Navier–Stokes equations; Reduced basis method

1 Introduction

In this paper, we consider two different FE approximations of the NSE arising from local projection-based methods for the LES of laminar and turbulent incompressible flows. The interest of the presented projection-based methods is that they allow an important reduction on the computational time requirements with respect to classical methodologies, providing at the same time high-order accuracy with reduced computational complexity. First, we introduce a full order model, which is a variant of standard LPS schemes, for the evolution NSE. The most relevant feature from the practical point of view is that the proposed full order approach looks simple overall, yet it manages to solve complex high Reynolds numbers flows on relatively coarse grids. Then, to further reduce computational complexity, we also consider a reduced order model, which consists of a RB VMS-Smagorinsky turbulence model, for the steady NSE (its extension to evolution NSE through its combination

with a proper orthogonal decomposition strategy is today in progress). The most relevant feature from the practical point of view is that the proposed reduced order approach yields a dramatic speed-up of the computing time with respect to the corresponding high fidelity model, while maintaining a similar accuracy up to moderate Reynolds numbers.

On the one hand, we focus on the high-order term-by-term stabilization method introduced in (*cf.* [1]) for the Oseen equations. This method is developed by a purely numerical approach that does not require any ad-hoc eddy viscosity. It is a particular type of LPS scheme, which constitutes a low-cost, accurate solver for incompressible flows, despite being only weakly consistent since it does not involve the full residual. It differs from the standard LPS methods (*cf.* [2, 3]) because it uses continuous buffer functions, it does not need enriched FE spaces, it does not need element-wise projections satisfying suitable orthogonality properties, and it does not need multiple meshes. Commonly to standard LPS methods, the stabilization terms only act on the small scales of the flow, thus ensuring a higher accuracy with respect to more classical stabilization procedures, such as penalty-stabilized methods (*cf.* [4]). This method has been recently supported by a thorough numerical analysis (existence and uniqueness, stability, convergence, error estimates, asymptotic energy balance) for the nonlinear problem related to the evolution NSE (*cf.* [5, 6]), using a semi-implicit Euler scheme for the monolithic discretization in time. The main results from the numerical analysis of the proposed LPS method will be recalled here. We will also focus on an efficient time discretization of this method via a stable velocity-pressure segregation, using semi-implicit Backward Differentiation Formulas up to the second order (BDF2), with a special emphasis on its numerical solution in a parallel setting (*cf.* [7]). We show some relevant 3D numerical tests, to assess the performance of the proposed LPS method as an efficient and accurate solver for the simulation of laminar and turbulent incompressible complex flows that could arise in industrial applications.

On the other hand, we present a promising RB VMS-Smagorinsky turbulence model, based upon the approximation of the sub-grid eddy viscosity term by means of the empirical interpolation method, and on the approximation of velocity-pressure by a Greedy algorithm built with a specific error estimator. The numerical analysis for the steady NSE is performed. Also, we present some numerical results for the benchmark 2D lid-driven cavity flow problem that show a dramatic speed-up of the computing time. The adaptation of this solver to complex flows, now in progress, is of primary interest for analysis and optimal design in fluid mechanics industrial applications.

The paper is organized as follows. In Sect. 2, we describe the proposed LPS approximation of the incompressible evolution NSE, commonly referred as high-order term-by-term stabilization, and we state its main properties. After recalling the main results from the numerical analysis of the proposed LPS method, we present an efficient and accurate time discretization of this model by means of an incremental pressure-correction algorithm with semi-implicit BDF2, and describe the parallel solver developed for the fully discrete problem. In Sect. 3, we show numerical studies to assess the performance of the proposed LPS strategy. In Sect. 4, the proposed RB VMS-Smagorinsky model for the steady NSE is introduced and theoretically analyzed. Numerical studies for this model are carried out in Sect. 5. In particular, the high computational efficiency of the proposed RB VMS-Smagorinsky model is showcased. Finally, Sect. 6 states the main conclusions of the paper.

2 A high-order LPS discretization of evolution NSE

We introduce a numerical approximation for an Initial-Boundary Value Problem (IBVP) describing the incompressible evolution NSE. For the sake of simplicity, we just impose homogeneous Dirichlet boundary condition on the whole boundary. More general inflow boundary conditions may be taken into account by standard lifting techniques for NSE. Also, the treatment of general non-linear wall law boundary conditions may be found in [8].

Let $[0,T]$ be the time interval, and Ω a bounded polyhedral domain in $\mathbb{R}^d$, $d = 2$ or 3, with a Lipschitz-continuous boundary $\Gamma = \partial\Omega$. Let $\{\mathcal{T}_h\}_{h>0}$ be a family of affine-equivalent, conforming (i.e., without hanging nodes) and regular triangulations of $\overline{\Omega}$, formed by triangles ($d = 2$) or tetrahedra ($d = 3$).

Given an integer $l \geq 2$ and a mesh cell $K \in \mathcal{T}_h$, denote by $\mathbb{P}_l(K)$ the space of polynomials of degree $\leq l$, defined on K. We consider the following FE spaces for the velocity:

$$\begin{cases} Y_h^l = V_h^l(\Omega) = \{v_h \in C^0(\overline{\Omega}) : v_h|_K \in \mathbb{P}_l(K), \forall K \in \mathcal{T}_h\}, \\ \mathbf{Y}_h^l = [Y_h^l]^d = \{\mathbf{v}_h \in [C^0(\overline{\Omega})]^d : \mathbf{v}_h|_K \in [\mathbb{P}_l(K)]^d, \forall K \in \mathcal{T}_h\}, \\ \mathbf{X}_h = \mathbf{Y}_h^l \cap \mathbf{H}_0^1(\Omega). \end{cases} \tag{1}$$

We approximate the weak formulation of the unsteady NSE by a high-order term-by-term stabilization procedure in space (*cf.* [1]). For simplicity of the analysis, we initially consider a semi-implicit Euler scheme for the monolithic discretization in time. To state it, consider a positive integer number N and define $\Delta t = T/N$, $t_n = n\Delta t$, $n = 0, 1, \ldots, N$. We compute the approximations $\mathbf{u}_h^n$, p_h^n to $\mathbf{u}^n = \mathbf{u}(\cdot, t_n)$ and $p^n = p(\cdot, t_n)$ by:

- *Initialization*. Set: $\mathbf{u}_h^0 = \mathbf{u}_{0h}$.
- *Iteration*. For $n = 0, 1, \ldots, N-1$: *Given* $\mathbf{u}_h^n \in \mathbf{X}_h$, *find* $(\mathbf{u}_h^{n+1}, p_h^{n+1}) \in \mathbf{X}_h \times \mathbb{M}_h$ *such that*:

$$\begin{cases} (\frac{\mathbf{u}_h^{n+1} - \mathbf{u}_h^n}{\Delta t}, \mathbf{v}_h)_\Omega + b(\mathbf{u}_h^n, \mathbf{u}_h^{n+1}, \mathbf{v}_h) + a(\mathbf{u}_h^{n+1}, \mathbf{v}_h) \\ \quad - (p_h^{n+1}, \nabla \cdot \mathbf{v}_h)_\Omega + s_{\text{conv}}(\mathbf{u}_h^n, \mathbf{u}_h^{n+1}, \mathbf{v}_h) + s_{\text{div}}(\mathbf{u}_h^{n+1}, \mathbf{v}_h) = \langle \overline{\mathbf{f}}^{n+1}, \mathbf{v}_h \rangle, \\ (\nabla \cdot \mathbf{u}_h^{n+1}, q_h)_\Omega + s_{\text{pres}}(p_h^{n+1}, q_h) = 0, \end{cases} \tag{2}$$

  for any $(\mathbf{v}_h, q_h) \in \mathbf{X}_h \times \mathbb{M}_h$, where $\mathbb{M}_h = Y_h^l \cap L_0^2(\Omega)$, $\overline{\mathbf{f}}^{n+1}$ is the average value of $\mathbf{f}$ in $[t_n, t_{n+1}]$, and $\mathbf{u}_{0h}$ is some stable approximation to $\mathbf{u}_0$ belonging to $\mathbf{X}_h$, e.g., its discrete Stokes projection.

The forms a and b in (2) are given by:

$$b\big(\mathbf{u}_h^n, \mathbf{u}_h^{n+1}, \mathbf{v}_h\big) = \frac{1}{2}\Big[\big(\mathbf{u}_h^n \cdot \nabla \mathbf{u}_h^{n+1}, \mathbf{v}_h\big)_\Omega - \big(\mathbf{u}_h^n \cdot \nabla \mathbf{v}_h, \mathbf{u}_h^{n+1}\big)_\Omega\Big], \tag{3}$$

$$a\big(\mathbf{u}_h^{n+1}, \mathbf{v}_h\big) = 2\nu\big(D\big(\mathbf{u}_h^{n+1}\big), D(\mathbf{v}_h)\big)_\Omega, \tag{4}$$

where $D(\mathbf{u})$ is the symmetric deformation tensor.

The forms s_{conv}, s_{div} and s_{pres} in (2) correspond to a high-order term-by-term stabilized method (*cf.* [1]), and are given by:

$$s_{\text{conv}}\big(\mathbf{u}_h^n, \mathbf{u}_h^{n+1}, \mathbf{v}_h\big) = \sum_{K \in \mathcal{T}_h} \tau_{v,K}\big(\sigma_h^*\big(\mathbf{u}_h^n \cdot \nabla \mathbf{u}_h^{n+1}\big), \sigma_h^*\big(\mathbf{u}_h^n \cdot \nabla \mathbf{v}_h\big)\big)_K, \tag{5}$$

$$s_{\mathrm{div}}\big(\mathbf{u}_h^{n+1},\mathbf{v}_h\big)=\sum_{K\in\mathcal{T}_h}\tau_{d,K}\big(\sigma_h^*\big(\nabla\cdot\mathbf{u}_h^{n+1}\big),\sigma_h^*(\nabla\cdot\mathbf{v}_h)\big)_K, \tag{6}$$

$$s_{\mathrm{pres}}\big(p_h^{n+1},q_h\big)=\sum_{K\in\mathcal{T}_h}\tau_{p,K}\big(\sigma_h^*\big(\nabla p_h^{n+1}\big),\sigma_h^*(\nabla q_h)\big)_K. \tag{7}$$

Here, $\tau_{v,K}$, $\tau_{d,K}$ and $\tau_{p,K}$ are stabilization coefficients for convection, divergence and pressure gradient, respectively, and $\sigma_h^*=\mathrm{Id}-\sigma_h$, where σ_h is some locally stable projection or interpolation operator from $\mathbf{L}^2(\Omega)$ on the foreground vector-valued space $\mathbf{Y}_h^{l-1}$ (also called "buffer space" in this context), satisfying optimal error estimates. In practical implementations, the stabilization coefficients are given by the Codina's form [9], designed by asymptotic scaling arguments applied in the framework of stabilized methods aimed at taking into account the local balance between convection and diffusion. Also, we choose σ_h as a Scott–Zhang-like [10] linear interpolation operator in the space $\mathbf{Y}_h^{l-1}$ (see [1], Sect. 4 for its construction), implemented in the software FreeFem++ [11]. This is an interpolator that just uses nodal values, and so is simpler to work out and more computationally efficient than variants requiring for instance integration on mesh elements (see, e.g., [12]). In formula (6), σ_h denotes an operator between the scalar spaces L^2 and Y_h^{l-1}, but we use the same notation for the sake of simplicity. Actually, if needed, specific stabilizations for convection, divergence and pressure gradient may be used, through different approximation operators.

2.1 Numerical analysis

The discrete method (2) has been recently supported by a thorough numerical analysis (stability, convergence, error estimates, asymptotic energy balance) for the nonlinear problem related to the evolution NSE (*cf.* [5, 6]), which is to our knowledge unavailable for most turbulence models in the current literature (*cf.* [13]).

Here, we recall the main results obtained from the numerical analysis. First, we need the following technical hypothesis on the stabilization coefficients:

Hypothesis 2.1 The stabilization coefficients $\tau_{p,K}$, $\tau_{d,K}$ and $\tau_{v,K}$ satisfy the following conditions:

$$\alpha_1 h_K^2\le\tau_{p,K}\le\alpha_2 h_K^2,\qquad 0<\tau_{d,K}\le\beta,\qquad 0<\tau_{v,K}\le\gamma h_K^2, \tag{8}$$

for all $K\in\mathcal{T}_h$, and some positive constants α_1, α_2, β, γ independent of h.

We next state a specific discrete inf-sup condition for the stabilized approximation that is essential for the stability of method (2).

Lemma 2.1 *Assume that Hypothesis* 2.1 *holds. Then, for a uniformly regular family of triangulations, we have the following inf-sup condition*:

$$\forall q_h\in\mathbb{M}_h,\quad \|q_h\|_{L^2}\le C\left(\sup_{\mathbf{v}_h\in\mathbf{X}_h}\frac{(\nabla\cdot\mathbf{v}_h,q_h)_\Omega}{\|D(\mathbf{v}_h)\|_{\mathbf{L}^2}}+\big\|\sigma_h^*(\nabla q_h)\big\|_{\tau_p}\right), \tag{9}$$

for some positive constant C independent of h, where τ_p denotes here the weighted L^2-norm with stabilization coefficient $\tau_{p,K}$.

The proof of this lemma can be derived from [1], where it is also shown that the discrete inf-sup condition (9) can be extended to a more complex condition that holds for a simply regular family of triangulations.

Let us now show results on existence, uniqueness of a solution and the stability of method (2). To state them, we shall consider the following discrete functions:

- $\mathbf{u}_h$ is the piecewise linear in time function with values on $\mathbf{X}_h$ such that $\mathbf{u}_h(t_n) = \mathbf{u}_h^n$,
- $\widetilde{p}_h$ is the piecewise constant in time function that takes the value p_h^{n+1} on (t_n, t_{n+1}),
- $P_h(t) = \int_0^t \widetilde{p}_h(s)\, ds$.

For simplicity of notation, we do not make explicit the dependence of these functions upon Δt.

Theorem 2.1 *Assume that Hypothesis* 2.1 *holds, and let* $\mathbf{f} \in L^2(\mathbf{H}^{-1})$, $\mathbf{u}_0 \in \mathbf{L}^2$. *Then, problem* (2) *admits a unique solution that satisfies the estimate*:

$$\|\mathbf{u}_h\|_{L^\infty(\mathbf{L}^2)} + \sqrt{\nu}\big\|D(\mathbf{u}_h)\big\|_{L^2(\mathbf{L}^2)} + \|P_h\|_{L^\infty(L^2)} \le C\left(\|\mathbf{u}_0\|_{\mathbf{L}^2} + \frac{1}{\sqrt{\nu}}\|\mathbf{f}\|_{L^2(\mathbf{H}^{-1})}\right), \tag{10}$$

where $C > 0$ *is a constant independent of* h *and* Δt.

The convergence of method (2) is now stated as follows:

Theorem 2.2 *Assume that Hypothesis* 2.1 *holds, and let* $\mathbf{f} \in L^2(\mathbf{H}^{-1})$, $\mathbf{u}_0 \in \mathbf{L}^2$. *Then, the sequence* $\{(\mathbf{u}_h, P_h)\}_{h>0}$ *contains a sub-squence* $\{(\mathbf{u}_{h'}, P_{h'})\}_{h'>0}$ *that is weakly convergent in* $L^2(\mathbf{H}^1) \times L^2(L^2)$ *to a weak solution* $(\mathbf{u}, P)$ *of the unsteady NSE, being* P *the time primitive of the physical pressure. Moreover,* $\{\mathbf{u}_{h'}\}_{h'>0}$ *is weakly-* convergent in* $L^\infty(\mathbf{L}^2)$ *to* $\mathbf{u}$, *strongly in* $L^2(\mathbf{H}^s)$ *for* $0 \le s < 1$, *and* $\{P_{h'}\}_{h'>0}$ *is weakly-* converegent in* $L^\infty(L^2)$ *to* P. *If the weak solution of the unsteady NSE is unique, then the whole sequence converges to it.*

The proofs of these theorems can be directly derived by the ones performed in [14].

We now state the following error estimate result:

Theorem 2.3 *Assume that Hypothesis* 2.1 *holds, the data verify* $\mathbf{f} \in C^0(\mathbf{H}^{-1})$, $\partial_t \mathbf{f} \in L^2(\mathbf{H}^{-1})$, $\mathbf{u}_0 \in \mathbf{H}^{s+1}$, *and that the solution* $(\mathbf{u}, p)$ *of the unsteady NSE has augmented regularity, i.e.,* $(\mathbf{u}, p) \in C^0(\mathbf{H}^{s+1}) \times C^0(H^s)$, $2 \le s \le l$, *such that* $\partial_{tt}\mathbf{u} \in L^2(\mathbf{L}^2)$. *Then, the following error estimate for a solution* $\{\mathbf{u}_h, p_h\}$ *of the fully discrete model* (2) *holds*:

$$\|\mathbf{u} - \mathbf{u}_h\|_{\ell^\infty(\mathbf{L}^2)} + \sqrt{\nu}\big\|D(\mathbf{u} - \mathbf{u}_h)\big\|_{\ell^2(\mathbf{L}^2)} + \|\widetilde{P} - P_h\|_{\ell^\infty(L^2)} \le C\big(h^s + \Delta t\big), \tag{11}$$

where $C > 0$ *is a constant independent of* h *and* Δt, *and we are using the following notation*:

$$\|\mathbf{u} - \mathbf{u}_h\|_{\ell^\infty(\mathbf{L}^2)} = \max_{n=1,\dots,N}\big\|\mathbf{u}^n - \mathbf{u}_h^n\big\|_{\mathbf{L}^2},$$

$$\big\|D(\mathbf{u} - \mathbf{u}_h)\big\|_{\ell^2(\mathbf{L}^2)} = \left[\sum_{n=1}^{N} \Delta t\big\|D\big(\mathbf{u}^n - \mathbf{u}_h^n\big)\big\|_{\mathbf{L}^2}^2\right]^{1/2},$$

$$\|\widetilde{P} - P_h\|_{\ell^\infty(L^2)} = \max_{n=1,\dots,N}\big\|\widetilde{P}^n - P_h^n\big\|_{L^2},$$

being $\widetilde{P} = \int_0^t \widetilde{p}(\cdot, s)\, ds$, *with* $\widetilde{p}$ *the piecewise constant in time function that takes the value* p^{n+1} *on* (t_n, t_{n+1}), *and* $\widetilde{P}^n = \widetilde{P}(\cdot, t_n)$, $P_h^n = P_h(t_n)$.

A detailed proof of this theorem can be found in [5]. Taking $s = l$, if the flow is regular enough, we obtain convergence of optimal order, and the order decreases with the regularity.

Remark 2.1 The proof of Theorem 2.3, that implies more concretely a strong convergence result for solutions with slightly increased regularity (it is sufficient $(\mathbf{u}, p) \in C^0(\mathbf{H}^2) \times C^0(H^1)$, even if the convergence order in space is limited to one, due to the pressure stabilizing term), contains as a sub-product the asymptotic energy balance of the approximation (2): the total energy balance is asymptotically maintained in such a way that the sub-grid energy due to stabilizing terms asymptotically vanish (see [15], Sect. 3.4). This is not the case if we consider the natural minimal regularity of the continuous solution: indeed, due to the low regularity of the weak solution, we can just prove an energy inequality, due to the dissipative nature of the approximation (2), by using that the sub-grid stabilizing energy terms are positive (*cf.* [14]).

Remark 2.2 The presented analysis for the proposed high-order term-by-term stabilization procedure has been extended to geophysical flows governed by the primitive equations of the ocean [16] and buoyant flows governed by the Boussinesq equations [17]. Also, it has been combined with a Variational Multi-Scale (VMS)-Smagorinsky term and wall laws for the accurate simulation of turbulent boundary layers in [14, 15, 18].

2.2 An efficient time discretization of the NSE with LPS modeling in a HPC framework

In this section, we propose to compute the approximations $\mathbf{u}_h^n$ and p_h^n by using an incremental pressure-correction scheme based on semi-implicit BDF, for which the nonlinear terms are extrapolated by means of Newton–Gregory backward polynomials. Let us denote by $\widetilde{\mathbf{u}}_h^n$ an intermediate approximate velocity at time t_n. In order to abbreviate its discrete time derivative, we define the operator D_t by:

$$D_t^r \widetilde{\mathbf{u}}_h^n := \frac{\alpha_r \widetilde{\mathbf{u}}_h^{n+1} - \widetilde{\mathbf{u}}_{h,r}^n}{\Delta t}, \tag{12}$$

where for BDF schemes of orders $r = 1, 2$ we have:

$$\widetilde{\mathbf{u}}_{h,r}^n = \begin{cases} \widetilde{\mathbf{u}}_h^n & \text{if } n \geq 0, \text{for } r = 1 \quad \text{(BDF1)}, \\ 2\widetilde{\mathbf{u}}_h^n - \frac{1}{2}\widetilde{\mathbf{u}}_h^{n-1} & \text{if } n \geq 1, \text{for } r = 2 \quad \text{(BDF2)} \end{cases} \tag{13}$$

and

$$\alpha_r = \begin{cases} 1, & \text{for } r = 1 \quad \text{(BDF1)}, \\ \frac{3}{2}, & \text{for } r = 2 \quad \text{(BDF2)}. \end{cases} \tag{14}$$

We consider the following extrapolations of order $r = 1, 2$ for the intermediate convection velocity:

$$\widetilde{\mathbf{u}}_{h,r}^{n,*} = \begin{cases} \widetilde{\mathbf{u}}_h^n & \text{if } n \geq 0, \text{for } r = 1 \quad \text{(BDF1)}, \\ 2\widetilde{\mathbf{u}}_h^n - \widetilde{\mathbf{u}}_h^{n-1} & \text{if } n \geq 1, \text{for } r = 2 \quad \text{(BDF2)} \end{cases} \tag{15}$$

and the pressure:

$$p_{h,r}^{n,*} = \begin{cases} p_h^n & \text{if } n \geq 0, \text{for } r = 1 \quad \text{(BDF1)}, \\ \frac{1}{3}(7p_h^n - 5p_h^{n-1} + p_h^{n-2}) & \text{if } n \geq 1, \text{for } r = 2 \quad \text{(BDF2)} \end{cases} \tag{16}$$

using in the last case the convention $p_h^{n-1} = p_h^{n-2}$ for $n = 1$. In this way, after applying a standard incremental pressure-correction approach (*cf.* [19] for derivation), the fully discrete semi-implicit formulation consists in solving, for $n = 0, \ldots, N-1$, the two-step algorithm:

find $\widetilde{\mathbf{u}}_h^{n+1} \in \mathbf{X}_h$ *such that*:

$$\begin{cases} (D_t^r \widetilde{\mathbf{u}}_h^n, \mathbf{v}_h)_\Omega + b(\widetilde{\mathbf{u}}_{h,r}^{n,*}, \widetilde{\mathbf{u}}_h^{n+1}, \mathbf{v}_h) + a(\widetilde{\mathbf{u}}_h^{n+1}, \mathbf{v}_h) + s_{\text{conv}}(\widetilde{\mathbf{u}}_{h,r}^{n,*}, \widetilde{\mathbf{u}}_h^{n+1}, \mathbf{v}_h) \\ \quad + s_{\text{div}}(\widetilde{\mathbf{u}}_h^{n+1}, \mathbf{v}_h) = \langle \overline{\mathbf{f}}^{n+1}, \mathbf{v}_h \rangle + (p_{h,r}^{n,*}, \nabla \cdot \mathbf{v}_h)_\Omega, \end{cases} \tag{17}$$

for any $\mathbf{v}_h \in \mathbf{X}_h$, where $\overline{\mathbf{f}}^{n+1}$ is the average value of $\mathbf{f}$ in $[t_n, t_{n+1}]$, and:

find $p_h^{n+1} \in \mathbb{M}_h$ *such that*:

$$\begin{cases} (\nabla(p_h^{n+1} - p_h^n), \nabla q_h)_\Omega + s_{\text{pres}}(p_h^{n+1}, q_h) = -\frac{\alpha_r}{\Delta t}(\nabla \cdot \widetilde{\mathbf{u}}_h^{n+1}, q_h)_\Omega, \\ (\mathbf{n} \cdot \nabla(p_h^{n+1} - p_h^n))_{|\Gamma} = 0, \end{cases} \tag{18}$$

for any $q_h \in \mathbb{M}_h$, where $\mathbf{n}$ is the outer normal to Γ.

The final velocity can then be recovered according to:

$$\mathbf{u}_h^{n+1} = \widetilde{\mathbf{u}}_h^{n+1} - \frac{\Delta t}{\alpha_r} \nabla \left(p_h^{n+1} - p_h^n \right). \tag{19}$$

In practical implementations, for the first time step ($n = 0$) we use a BDF1 scheme ($r = 1$) to initialize the algorithm with $\widetilde{\mathbf{u}}_h^0 = \mathbf{u}_h^0$ and p_h^0 some stable approximations to $\mathbf{u}^0$ and p^0, respectively. Note that this scheme coincides with the semi-implicit Euler method (2). Then, a BDF2 scheme ($r = 2$) is applied for $n \geq 1$.

The semi-implicit discretization in time segregating velocity and pressure through a standard incremental time-splitting helps to construct an efficient linear solver to the NSE system for the LES of laminar and turbulent incompressible flows. In the first step (17), a convection-dominated convection–diffusion–reaction subproblem for the intermediate velocity must be solved. The second step (18) consists of a stabilized pressure-Poisson subproblem. Solving the associated large linear systems could become extremely expensive from the computational point of view, that is why we adopt in the numerical implementation a highly parallel strategy based on Domain Decomposition Methods (DDM). Both steps are solved by using a DDM preconditioner with the GMRES iterative method applied to the associated system in the parallel framework described in [7], and a convincing strong scaling analysis of the used algorithm is showcased in this framework. In particular, we have interfaced the proposed fully discrete scheme (17)–(18) with HPDDM [20, 21], a high performance unified framework for DDM, and used a parallel iterative linear solver based on an optimized Schwarz DDM as preconditioner [20, 22]. In this manner, we obtain an efficient, i.e., robust and fast, solver for the High Performance Computing (HPC) of laminar and turbulent incompressible flows in the open-source FE software FreeFem++ interfaced with the library HPDDM. The proposed parallel strategy is tested for the recirculating flow in a 3D lid-driven cavity in the next section.

3 Numerical experiments with LPS by interpolation method

In this section, we discuss some numerical results to analyze the numerical performances of the proposed LPS model applied to the computation of laminar and turbulent complex flows that could arise in industrial applications, also on massive parallel settings.

3.1 Turbulent channel flow (3D)

We present results of a fully developed turbulent flow in a 3D channel at moderate friction Reynolds number $Re_\tau = 180$. The 3D channel flow is one of the most popular test problems for the investigation of wall bounded turbulent flows, whereas turbulent boundary layers are of high practical relevance in aerodynamics industries. The proposed test consists of a fluid that flows between two parallel walls driven by an imposed pressure gradient source term which is defined by the friction Reynolds number Re_τ. For the setup of our numerical simulations, we chose to follow the guidelines given by Gravemeier in [23]. As a benchmark, we will use the fine Direct Numerical Simulation (DNS) of Moser, Kim and Mansour [24].

The boundary conditions are periodic in both the stream-wise and span-wise directions (homogeneous directions). We perform a comparison between the application of the logarithmic wall-law of Prandtl and Von Kármán and no-slip boundary conditions at the walls.

We aim to obtain a good accuracy with a relatively coarse spatial resolution. The computational grid consists of a $16 \times 32 \times 16$ partition of the channel, uniform in the homogeneous directions. The distribution of nodes in the wall-normal direction is non-uniform, and obeys the cosine function of Gauss–Lobatto. We use 3D $\mathbb{P}_2$ FE for velocity and pressure.

We consider for this test a semi-implicit Crank–Nicolson scheme for the monolithic temporal discretization. This provides a good compromise between accuracy and computational complexity, while keeping the numerical diffusion levels below the sub-grid terms (*cf.* [25]). Indeed, on the one side, it produces less numerical diffusion with respect to a simple semi-implicit Euler scheme, and thus it does not tend to artificially increment the turbulent diffusion. On the other side, despite being a first-order method, it already provides accurate results at the considered moderate friction Reynolds number Re_τ, being less expensive in terms of storage requirements with respect to the two-step BDF2 scheme described in Sect. 2.2, which instead allows to achieve a second-order accuracy in time.

In Fig. 1 (left), we show the mean stream-wise velocity profiles, normalized by the computed wall shear velocity, in wall coordinates. The results show an acceptable agreement with the fine DNS, even with the very coarse basic discretization at hand (almost 4 times coarser than the DNS one).

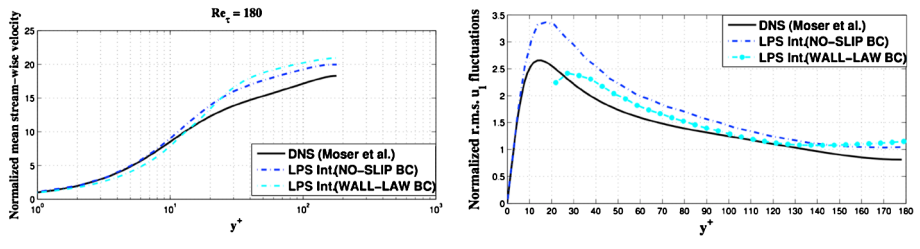

Figure 1 Example 3.1. Normalized mean stream-wise velocity profiles (left) and r.m.s. velocity fluctuations (right) in wall coordinates

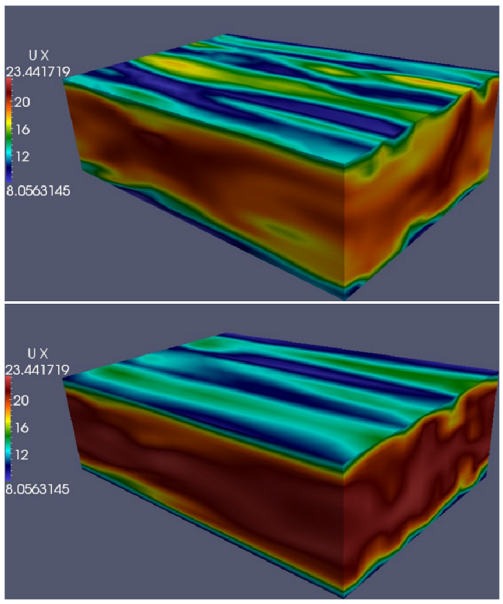

Figure 2 Example 3.1. Snapshot of stream-wise velocity contours at $t = 5$ (top) and $t = 10$ (bottom)

Figure 1 (right) displays the normalized r.m.s. values of the stream-wise velocity fluctuations. If we compare with DNS data the LPS method by interpolation tested with no-slip boundary conditions, we observe a noticeable over-prediction, which seems to be corrected by the use of wall laws in the so-called inertial layer, starting from the first interior node.

Figure 2 shows the stream-wise velocity contours at different instants in time, computed by the LPS method employing wall-law boundary conditions. Note the presence of turbulent structures (velocity fluctuations) on the wall-normal boundary inside the boundary layer (top surfaces), and as the flow becomes more homogenous as time increases, as physically expected.

Remark 3.1 Note that the present numerical study differs from the one performed in [14, 15, 18], where the combination with a VMS-Smagorinsky turbulence model has been considered on a computational grid that consists of a 16^3 partition of the channel. The presented results show that taking into account just a purely LPS method (no ad-hoc eddy viscosity of Smagorinsky-type is introduced) provides almost the same high-order accuracy of the more complex VMS-LPS method in [14, 15, 18], whenever we consider a proper refinement just on the wall-normal direction, giving results very close to the fine DNS.

3.2 Lid-driven cavity flow (3D)

In this section, the 3D lid-driven cavity test is performed to investigate the numerical performances of the proposed solver at laminar, transient, and turbulent regimes, also on massive parallel settings. The lid-driven cavity flow is one of the most studied problem in Computational Fluid Dynamics (CFD), that exhibits one direction of inhomogeneity. This problem is characterized by a fluid flow in a cubic domain driven by a tangential unitary velocity along one of the six boundary surfaces. Homogeneous Dirichlet conditions are adopted on all the other boundaries.

The recirculating flow in a 3D lid-driven cavity presents the occurrence of some considerable 3D features, even at relatively low Reynolds numbers. One of the most remarkable is the formation of Taylor–Görtler-like (TGL) vortices at the corners of the bottom of the cavity. Small counter-rotating vortices are formed as a result of the curvature of the streamlines due to the main vortex in the middle of the cavity. Following the work of Gravemeier et al. [26], we simulate the 3D cavity flow at Reynolds numbers $Re = 3200, 7500, 10{,}000$, to cover respectively the laminar, transient and turbulent regimes.

Also for this test, we first aim to obtain a good accuracy with a relatively coarse spatial resolution. The computational grid consists of a 32^3 partition of the unit cube, uniform in the y-direction, and refined towards the walls in both x- and z-directions using the hyperbolic tangent function, in order to handle large velocity gradients. Again, we use 3D $\mathbb{P}_2$ FE for velocity and pressure. For this test, we apply the efficient time discretization described in Sect. 2.2 in a parallel setting. Indeed, since we arrive to high Reynolds numbers, then the use of (at least) second-order accurate discretization in time has been found to be essential in order to achieve a reasonable accuracy. The results are graphically compared to the experimental data of Prasad and Koseff [27], and numerical results of Gravemeier et al. [26], obtained by a three-level VMS-Smagorinsky method (VMS-3L).

Figure 3 shows the mean velocities $\langle u_1 \rangle$ (left) and $\langle u_3 \rangle$ (right) respectively on the centerline $z = 0.5$ and $x = 0.5$ of the longitudinal mid-plane $y = 0.5$, for the various Reynolds numbers under consideration (top to bottom). The proposed method shows a good agreement with the experimental data of Prasad and Koseff [27], even with the coarse basic discretization at hand, and performs similarly (or even better) than the more complex VMS-3L method [26].

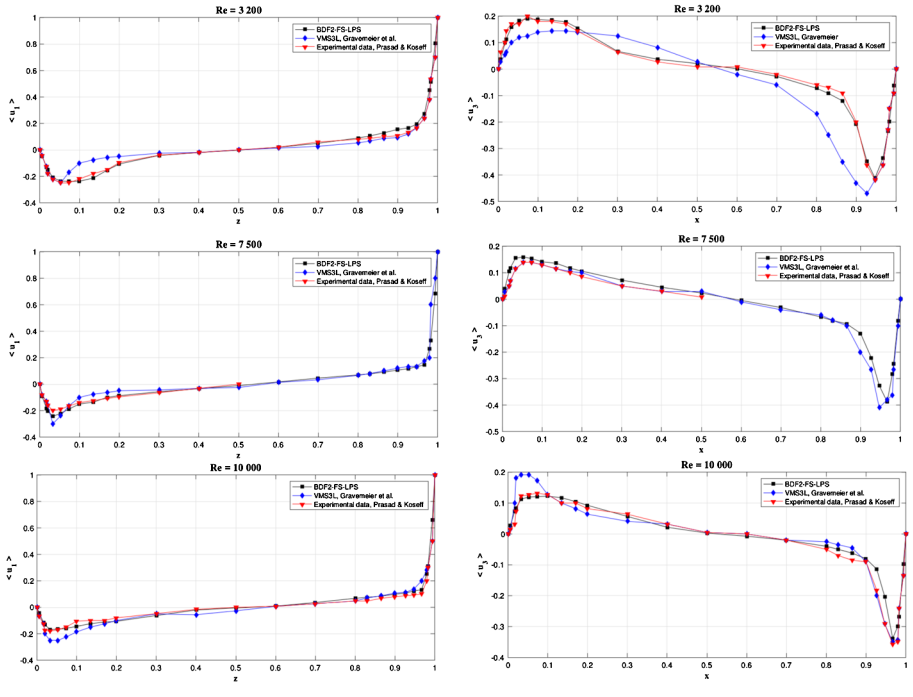

Figure 3 Example 3.2. Mean velocities profiles on the centerlines of the mid-plane $y = 0.5$ for $Re = 3200, 7500, 10{,}000$ (top to bottom)

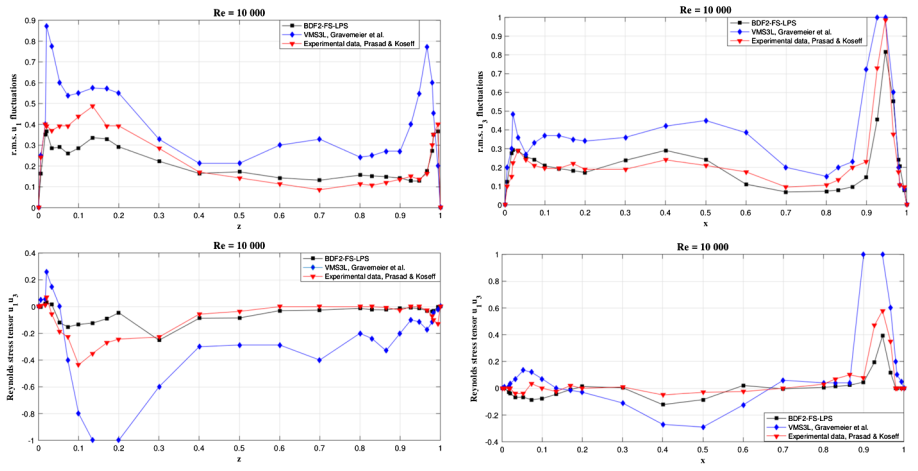

Figure 4 Example 3.2. R.m.s. velocity fluctuations (top) and Reynolds stress tensor (bottom) profiles on the centerlines of the mid-plane $y = 0.5$ for $Re = 10{,}000$

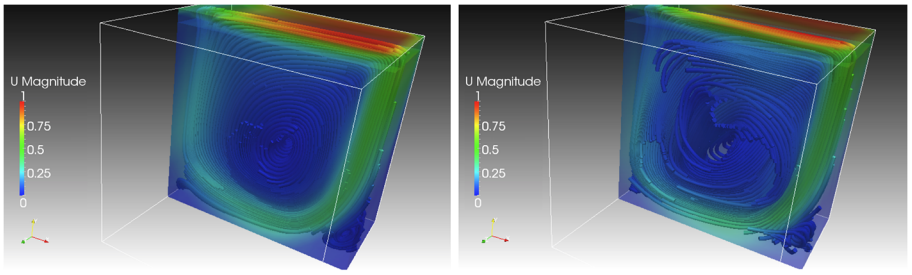

Figure 5 Example 3.2. Flow streamlines (colored by the velocity magnitude) at $Re = 3200$ (left) and $Re = 7500$ (right) for the proposed LPS method at final simulation time

Figure 4 displays the r.m.s. velocity fluctuations for the first and third component of the velocity (top), and the off-diagonal component of the Reynolds stress tensor (bottom), on the centerlines of the mid-plane $y = 0.5$ for $Re = 10{,}000$. As in Prasad and Koseff [27], the r.m.s. values and the off-diagonal Reynolds stress component are multiplied by the amplification factors 10 and 500, respectively, in order to ensure a reasonable visual impression of these values within the respective graphs. Also in predicting these sensitive measures, the proposed method shows a rather good agreement with the experimental data of Prasad and Koseff [27], and performs better than the VMS-3L method [26].

Qualitatively, we have observed that the flow exhibits effectively the formation of three-dimensional TGL corner vortices at the cavity end walls, that interact with the primary circulation vortex, thus influencing the distribution of momentum within the entire cavity, see Fig. 5. In the case $Re = 3200$, in accordance to Prasad and Koseff [27], it is possible to discern these vortices as organized structures, while for higher Re, increasing turbulent effects cause the breakdown of these organized structures. This suggests that the high-frequency turbulent fluctuations become dominant, and partially destroy the integrity (or coherence) of the TGL vortices.

Finally, to assess the parallel efficiency of the proposed method, we considered a very fine mesh using 100 grid points in each direction (24 million velocity unknowns and 8

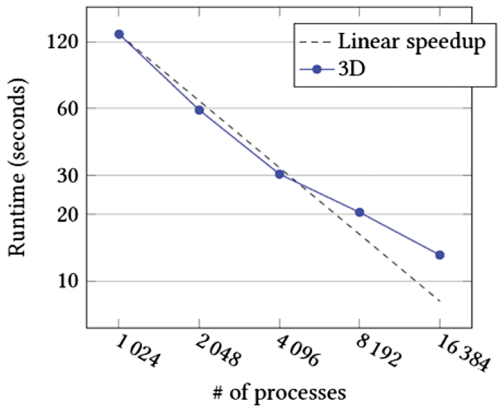

Figure 6 Example 3.2. Strong scaling analysis of the solver for $Re = 10{,}000$

Table 1 Example 3.2. Number of GMRES iterations of the solver for $Re = 10{,}000$

# of subdomains	# of velocity iterations	# of pressure iterations
1024	18	17
2048	19	12
4096	21	14
8192	24	15
16,384	23	13

millions pressure unknowns), and used from 1024 up to 16,384 MPI processes with a single OpenMP thread per process (flat MPI parallelism). Preconditioners are thus defined with as many subdomains as the number of MPI processes. We used the test case in the turbulent regime ($Re = 10{,}000$). In particular, we are interested in the strong scalability performances of the described algorithm. Results were obtained on Curie, a system composed of 5040 nodes with two eight-core Intel Sandy Bridge clocked at 2.7 GHz. Figure 6 represents the total average time to complete a time step. Clearly, the implementation scales very well, at least up to 4096 processes, where we start to notice a slight deterioration of the performance. Anyway, as displayed in Table 1, the preconditioners are both numerically extremely stable, with numbers of iterations remaining in the same low range. The GMRES method is stopped when the relative preconditioner residual is lower than 10^{-8} for the velocity unknows and 10^{-6} for the pressure unknows

Remark 3.2 Note that this numerical study differs from the one performed in [7], where just mixed inf-sup stable FE of Taylor–Hood type ($\mathbb{P}_2/\mathbb{P}_1$) have been considered for the pair velocity/pressure in numerical experiments, for which the pressure stabilized term (7) is neglected. The presented results with equal-order $\mathbb{P}_2/\mathbb{P}_2$ FE considering pressure stabilization are almost comparable with the ones of [7], thus being in good agreement with experimental data. However, the use of mixed FE leads to cheaper (amortized setup) Poisson solves for the pressure equation (18) in the HPC framework considered. This is reflected in Fig. 6, where we start to observe from 4096 processes that using equal-order FE leads to a slight deterioration in the scalability of the total average time to complete a time step, which is not the case when considering mixed FE in [7]. This follows from the fact that using equal-order FE requires the assembly of an additional term for pressure stabilization and, as consequence, this results in an increased computational cost with respect to mixed

formulations. Nevertheless, the number of GMRES iterations remains stable, and in the same low range as in Ref. [7] (see Table 1). To sum up, also the parallel performances in the case of equal-order FE are rather satisfactory, and seem to be in accordance with the current state-of-the-art, e.g., [28].

4 RB VMS-Smagorinsky model

In this section, we present a RB VMS-Smagorinsky turbulence model. This differs from the reduced order model considered in [29, 30], which is just based on the simpler Smagorinsky turbulence model. In particular, an interpolation operator has been introduced, in order to restrict the influence of the eddy viscosity just to the small resolved scales. This allows to avoid the over-diffusion phenomenon of the standard Smagorinsky model, where the effect of the un-resolved scales is typically taken into account equally for all resolved flow scales, and as a consequence, the large scales are usually over-damped, yielding results with lower accuracy, un-useful for most flows of practical interest in industry.

The idea supporting the RB method is to build a *reduced* basis formed by a few number of solutions from the original problem for some values of the parameter, in the *offline* phase. Then, the problem is solved by a Galerkin projection onto the space $\mathbf{X}_N \times \mathbb{M}_N$ spanned by the RB, in the *online* phase.

Let us introduce the space

$$\widetilde{\mathbf{X}_h} = \mathbf{Y}_h^{l-1} \cap \mathbf{H}_0^1(\Omega), \tag{20}$$

and consider a uniformly stable (in $H^1 - norm$) interpolation operator Π_h on $\widetilde{\mathbf{X}_h}$. This interpolation operator Π_h must satisfy optimal error estimates (*cf.* [31]), and preserve the boundary conditions when restricted to $\mathbf{X}_h$. Thus, we define

$$\mathbf{X}_h' = (\mathrm{Id} - \Pi_h)\mathbf{X}_h, \tag{21}$$

identifying $\widetilde{\mathbf{X}_h} = \Pi_h \mathbf{X}_h$ as the large velocity scales space, and $\mathbf{X}_h'$ the sub-filter scales velocities space. Space $\mathbf{X}_h'$ does not need to be explicitly constructed, only the operator Π_h is needed.

In our case, the parameter that we consider is the Reynolds number μ, assumed to range in a compact interval $\mathcal{D} \subset \mathbb{R}$. The finite element VMS-Smagorinsky model is given by:

$$\begin{cases} \text{Given } \mu \in \mathcal{D}, \text{find } (\mathbf{u}_h(\mu), p_h(\mu)) \in \mathbf{X}_h \times \mathbb{M}_h \text{ such that:} \\ \frac{1}{\mu}(\nabla \mathbf{u}_h, \nabla \mathbf{v}_h)_\Omega - (p_h, \nabla \cdot \mathbf{v}_h)_\Omega + (\nabla \cdot \mathbf{u}_h, q_h)_\Omega \\ \quad + (\mathbf{u}_h \cdot \nabla \mathbf{u}_h, \mathbf{v}_h)_\Omega + (\nu_T(\mathbf{u}_h')\nabla \mathbf{u}_h', \nabla \mathbf{v}_h')_\Omega = \langle \mathbf{f}, \mathbf{v}_h \rangle, \end{cases} \tag{22}$$

for any $(\mathbf{v}_h, q_h) \in \mathbf{X}_h \times \mathbb{M}_h$. Here we are denoting

$$\mathbf{u}_h' = (\mathrm{Id} - \Pi_h)\mathbf{u}_h, \qquad \mathbf{v}_h' = (\mathrm{Id} - \Pi_h)\mathbf{v}_h.$$

The eddy viscosity in the VMS-Smagorinsky model is defined as $\nu_T(\mathbf{u}_h') = (C_S h_K)^2 \times |\nabla \mathbf{u}_{h|K}'|$, where $|\cdot|$ denotes the Frobenius norm and C_S is the Smagorinsky constant. To linearise this non-linear term, we use the Empirical Interpolation Method (*cf.* [32]). This allows a large speed-up in the solution of the RB problem.

Remark 4.1 Problem (22) is supposed to have homogeneous Dirichlet boundary conditions. In the case of considering non-homogeneous Dirichlet boundary conditions, problem (22) is transformed to an equivalent one with homogeneous boundary conditions by considering a lift function. For more details, see e.g. [30, 33].

The idea to solve the VMS-Smagorinsky model by the RB method is the same to solve it by the FE method. We solve the VMS-Smagorinsky model by a Galerkin projection, but the main difference between FE and RB methods falls on the dimension of the spaces where we do the Galerkin projection. The RB space is low-dimensional, while the FE one is usually a high-dimensional space. We consider the RB VMS-Smagorinsky problem as

$$\begin{cases} \text{Given } \mu \in \mathcal{D}, \text{find } U_N(\mu) = (\mathbf{u}_N(\mu), p_N(\mu)) \in \overline{\mathbf{X}}_N = \mathbf{X}_N \times \mathbb{M}_N \text{ such that:} \\ A(U_N(\mu), V_N; \mu) = F(V_N; \mu) \quad \forall V_N \in \overline{\mathbf{X}}_N, \end{cases} \tag{23}$$

where we are denoting

$$\begin{aligned} A\big(U_N(\mu), V_N; \mu\big) = {} & \frac{1}{\mu} A_1(U_N, V_N) + A_2(U_N, V_N) \\ & + A_3(U_N, U_N, V_N) + A_4(U_N; U_N, V_N), \end{aligned} \tag{24}$$

with

$$\begin{aligned} & A_1(U_N, V_N) = (\nabla \mathbf{u}_N, \nabla \mathbf{v}_N)_\Omega, \\ & A_2(U_N, V_N) = -(p_N, \nabla \cdot \mathbf{v}_N)_\Omega + (\nabla \cdot \mathbf{u}_N, q_N)_\Omega, \\ & A_3(U_N, U_N, V_N) = (\mathbf{u}_N \cdot \nabla \mathbf{u}_N, \mathbf{v}_N)_\Omega, \\ & A_4(U_N; U_N, V_N) = \big(\nu_T\big(\mathbf{u}'_N\big)\nabla \mathbf{u}'_N, \nabla \mathbf{v}'_N\big)_\Omega, \end{aligned} \tag{25}$$

and $\mathbf{u}'_N = (\mathrm{Id} - \Pi_h)\mathbf{u}_N$. In the offline phase, to construct the reduced spaces we use the greedy algorithm. For the startup of the greedy algorithm we choose an arbitrary parameter value $\mu^1 \in \mathcal{D}$, and compute $(\mathbf{u}_h(\mu^1), p_h(\mu^1))$. The greedy algorithm recursively chooses the following snapshot for the reduced space as the value of the parameter that yields the maximum error between the high fidelity FE solution and the RB solution. As the computation of the exact error is quite expensive, we have built an *a posteriori* error bound estimator $\Delta_N(\mu)$, i.e., it selects the $(N+1)$th parameter value satisfying

$$\mu^{N+1} = \arg\max_{\mu \in \mathcal{D}} \Delta_N(\mu), \quad 1 \le N \le N_{\max}. \tag{26}$$

In this way, the reduced spaces for velocity and pressure are defined as

$$\mathbb{M}_N = \operatorname{span}\big\{\xi_k^p := p_h\big(\mu^k\big), k = 1, \ldots, N\big\}, \tag{27}$$

$$\mathbf{X}_N = \operatorname{span}\big\{\zeta_{2k-1}^{\mathbf{v}} := \mathbf{u}_h\big(\mu^k\big), \zeta_{2k}^{\mathbf{v}} := T_p^\mu \xi_k^p, k = 1, \ldots, N\big\}; \tag{28}$$

Here, T_p^μ is the so-called inner pressure *supremizer* operator $T_p^\mu : \mathbb{M}_h \to \mathbf{X}_h$, defined as $(T_p^\mu p_h, \mathbf{v}_h) = -(p_h, \nabla \cdot \mathbf{v}_h)_\Omega$, $\forall \mathbf{v}_h \in \mathbf{X}_h$, where $(\cdot, \cdot)$ is a scalar product in the velocity space $\mathbf{H}_0^1(\Omega)$. Adding the supremizers of the pressures to the reduced velocity space $\mathbf{X}_N$ ensures the stability of the discretization of the pressure in problem (23).

4.1 *A posteriori* error bound estimator

In this section, we present the tools for the construction of the *a posteriori* error bound estimator. For this purpose, we use the Brezzi-Rapaz-Raviart (BRR) theory (*cf.* [34]). Let us denote the directional derivative, at $U \in \overline{\mathbf{X}}_h = \mathbf{X}_h \times \mathbb{M}_h$, in the direction $Z = (\mathbf{z}, p_z) \in \overline{\mathbf{X}}_h$, as $\partial_1 A(U, \cdot; \mu)(Z)$. If we derive each operator term in (24), we obtain

$$\partial_1 A_1(U, V)(Z) = A_0(Z, V),$$

$$\partial_1 A_2(U, V)(Z) = A_1(Z, V),$$

$$\partial_1 A_3(U; V)(Z) = (\mathbf{u} \cdot \nabla \mathbf{z}, \mathbf{v})_\Omega + (\mathbf{z} \cdot \nabla \mathbf{u}, \mathbf{v})_\Omega,$$

$$\partial_1 A_4(U; V)(Z) = \left(\nu_T(\mathbf{u}')\nabla \mathbf{z}', \nabla \mathbf{v}'\right)_\Omega + \sum_{K \in \mathcal{T}_h} \int_K (C_S h_K)^2 \frac{\nabla \mathbf{u}' : \nabla \mathbf{z}'}{|\nabla \mathbf{u}'|} \left(\nabla \mathbf{u}' : \nabla \mathbf{v}'\right) d\Omega.$$

For the well posedness of the problem, we have to guarantee the uniform coerciveness and the boundedness of $\partial_1 A$ in the sense that for any solution $U_h(\mu)$ of (22), there exist $\beta_0 > 0$ and $\gamma_0 \in \mathbb{R}$ such that $\forall \mu \in \mathcal{D}$,

$$\begin{aligned} 0 < \beta_0 < \beta_h(\mu) &\equiv \inf_{Z_h \in \overline{\mathbf{X}}_h} \sup_{V_h \in \overline{\mathbf{X}}_h} \frac{\partial_1 A(U_h(\mu), V_h; \mu)(Z_h)}{\|Z_h\|_{\overline{\mathbf{X}}_h} \|V_h\|_{\overline{\mathbf{X}}_h}}, \\ \infty > \gamma_0 > \gamma_h(\mu) &\equiv \sup_{Z_h \in \overline{\mathbf{X}}_h} \sup_{V_h \in \overline{\mathbf{X}}_h} \frac{\partial_1 A(U_h(\mu), V_h; \mu)(Z_h)}{\|Z_h\|_{\overline{\mathbf{X}}_h} \|V_h\|_{\overline{\mathbf{X}}_h}}. \end{aligned} \tag{29}$$

Then, according to the BRR theory (*cf.* [34, 35]), it will follow that in a neighbourhood of $U_h(\mu)$ the solution of (22) is unique and bounded in $\|\cdot\|_{\overline{\mathbf{X}}_h}$ in terms of the data. The proof of the existence of $\beta_h(\mu)$ can be derived from Proposition 4.2 of [30], thanks to the fact that the interpolation operator Π_h satisfies optimal error estimates (*cf.* [31]).

For the development of the *a posteriori* error bound, we start by proving that the directional derivative of the operator $A(\cdot, \cdot; \mu)$ is globally lipschitz. The proof of the following Lemma can be derived from Lemma 5.1 in [30].

Lemma 4.1 *There exists a positive constant ρ_T such that, $\forall U_h^1, U_h^2, Z_h, V_h \in \overline{\mathbf{X}}_h$,*

$$|\partial_1 A\left(U_h^1, V_h; \mu\right)(Z_h) - \partial_1 A\left(U_h^2, V_h; \mu\right)(Z_h)| \leq \rho_T \left\|U_h^1 - U_h^2\right\|_{\overline{\mathbf{X}}_h} \|Z_h\|_{\overline{\mathbf{X}}_h} \|V_h\|_{\overline{\mathbf{X}}_h}. \tag{30}$$

The following continuity and inf-sup conditions hold:

$$\infty > \gamma_N(\mu) \equiv \sup_{Z_h \in \overline{\mathbf{X}}_h} \sup_{V_h \in \overline{\mathbf{X}}_h} \frac{\partial_1 A(U_N(\mu), V_h; \mu)(V_h)}{\|Z_h\|_{\overline{\mathbf{X}}_h} \|V_h\|_{\overline{\mathbf{X}}_h}}, \tag{31}$$

$$0 < \beta_N(\mu) \equiv \inf_{Z_h \in \overline{\mathbf{X}}_h} \sup_{V_h \in \overline{\mathbf{X}}_h} \frac{\partial_1 A(U_N(\mu), V_h; \mu)(Z_h)}{\|Z_h\|_{\overline{\mathbf{X}}_h} \|V_h\|_{\overline{\mathbf{X}}_h}}. \tag{32}$$

The suitability of the *a posteriori* error bound estimator is stated by the following results. Their proofs can be derived from [30], taking into account that the interpolation operator Π_h is uniformly stable in H^1-norm.

Theorem 4.1 *Let $\mu \in \mathcal{D}$, and assume that $\beta_N(\mu) > 0$. If problem* (22) *admits a solution $U_h(\mu)$ such that*

$$\big\| U_h(\mu) - U_N(\mu) \big\|_{\overline{\mathbf{X}}_h} \leq \frac{\beta_N(\mu)}{\rho_T},$$

then this solution is unique in the ball $B_{\overline{\mathbf{X}}_h}(U_N(\mu), \frac{\beta_N(\mu)}{\rho_T})$.

Let us define the *a posteriori* error bound estimator by

$$\Delta_N(\mu) = \frac{\beta_N(\mu)}{2\rho_T}\big[1 - \sqrt{1 - \tau_N(\mu)}\big], \tag{33}$$

where $\tau_N(\mu)$ is given by

$$\tau_N(\mu) = \frac{4\epsilon_N(\mu)\rho_T}{\beta_N^2(\mu)}, \tag{34}$$

with $\epsilon_N(\mu)$ the dual norm of the residual

$$\epsilon_N(\mu) = \big\| \mathcal{R}\big(U_N(\mu); \mu\big) \big\|_{\overline{\mathbf{X}}_h'}. \tag{35}$$

Theorem 4.2 *Assume that $\beta_N(\mu) > 0$ and $\tau_N(\mu) \leq 1$ for all $\mu \in \mathcal{D}$. Then there exists a unique solution $U_h(\mu)$ of* (22) *such that the error with respect $U_N(\mu)$, solution of* (23)*, is bounded by the a posteriori error bound estimator, i.e.,*

$$\big\| U_h(\mu) - U_N(\mu) \big\|_{\overline{\mathbf{X}}_h} \leq \Delta_N(\mu), \tag{36}$$

with effectivity

$$\Delta_N(\mu) \leq \left[\frac{2\gamma_N(\mu)}{\beta_N(\mu)} + \tau_N(\mu)\right] \big\| U_h(\mu) - U_N(\mu) \big\|_{\overline{\mathbf{X}}_h}. \tag{37}$$

5 Numerical experiments with RB VMS-Smagorinsky method

In this section we present numerical results for the RB VMS-Smagorinsky model. We consider the 2D lid-driven cavity problem, with Reynolds number ranging in $\mu \in [1000, 5100]$. In the offline phase, we compute the FE approximation with Taylor–Hood FE pairs. We consider a regular mesh with 5000 triangles and 2601 nodes. The FE steady state solution is computed through a semi-implicit evolution approach (the semi-implicit Euler method is used for simplicity), and we conclude that the steady solution is reached when the relative error between two iterators is below $\varepsilon_{\mathrm{FE}} = 10^{-10}$. The numerical scheme to solve the full order VMS-Smagorinsky model in each time step reads

$$\begin{cases} \text{Find } (\mathbf{u}_h^{n+1}(\mu), p_h^{n+1}(\mu)) \in \mathbf{X}_h \times \mathbb{M}_h \text{ such that } \forall \mathbf{v}_h \in \mathbf{X}_h, \forall q_h \in \mathbb{M}_h\text{:} \\ (\frac{\mathbf{u}_h^{n+1} - \mathbf{u}_h^n}{\Delta t})_\Omega + \frac{1}{\mu}(\nabla \mathbf{u}_h^{n+1}, \nabla \mathbf{v}_h)_\Omega - (p_h^{n+1}, \nabla \cdot \mathbf{v}_h)_\Omega \\ \quad + (\nabla \cdot \mathbf{u}_h^{n+1}, q_h)_\Omega + (\mathbf{u}_h^n \cdot \nabla \mathbf{u}_h^{n+1}, \mathbf{v}_h)_\Omega \\ \quad + (\nu_T(\mathbf{u}_h'^n) \nabla \mathbf{u}_h'^{n+1}, \nabla \mathbf{v}_h')_\Omega = \langle \mathbf{f}, \mathbf{v}_h \rangle. \end{cases} \tag{38}$$

In order to implement the VMS-Smagorinsky eddy diffusion, we consider a standard nodal Lagrange interpolation operator for its simplicity and efficiency with respect to other choices. First, to start the Greedy algorithm, we set up the Empirical Interpolation Method in order to approximate the eddy viscosity term. We need 34 basis functions until reaching the tolerance for the error in the Empirical Interpolation Method, see [30] for more details.

We start the Greedy algorithm for $\mu = 1000$, and we need $N = 9$ basis functions until reaching the Greedy tolerance of 10^{-5} for the *a posteriori* error bound estimator. Since the VMS-Smagorinsky model is less diffusive than the classical Smagorinsky model, the number of basis functions needed for the RB model is lower. In [30] where a classical Smagorinsky model is considered, for the same numerical test, the Greedy algorithm selects 12 basis functions instead of 9 basis functions.

In Fig. 7, we can observe the evolution of the *a posteriori* error bound within the Greedy algorithm. Due to Theorem 4.2, $\Delta_N(\mu)$ exists when $\tau_N(\mu) \leq 1$. While $\tau_N(\mu) > 1$, we use as *a posteriori* error bound estimator the proper $\tau_N(\mu)$. We stop the Greedy algorithm when we reach a tolerance of $\varepsilon_{RB} = 10^{-5}$.

In Fig. 8, we show the value of the *a posteriori* error bound estimator and the relative error for all $\mu \in \mathcal{D}$, at $N = N_{\max}$. We observe that it is indeed a good error estimator, with an efficiency factor lower of 10 for all $\mu \in \mathcal{D}$. This efficiency is improved from the lid-driven cavity test presented in [30].

In Fig. 9, we show a comparison between the FE velocity solution (left) and the RB velocity solution (right) for a chosen parameter value $\mu = 2142$. We observe that primary and secondary vortices are well-resolved in both cases. Note that both images are practically equal, as the error between both solutions is of order 10^{-6}.

In Table 2, we show the results obtained for several values of μ in $\mathcal{D}$. The FE problem has 23,003 degrees of freedom, while the RB problem has 27 degrees of freedom, plus 34 degrees of freedom for the Empirical Interpolation Method. We observe a dramatic reduction of the computational time, of several thousands, with errors below the Greedy tolerance. The speed-up obtained in this test is greater than in the lid-driven cavity test presented in [30] for the classical Smagorinsky model, since the computational time for a FE VMS-Smagorinsky solution is greater than the computational time for a FE Smagorin-

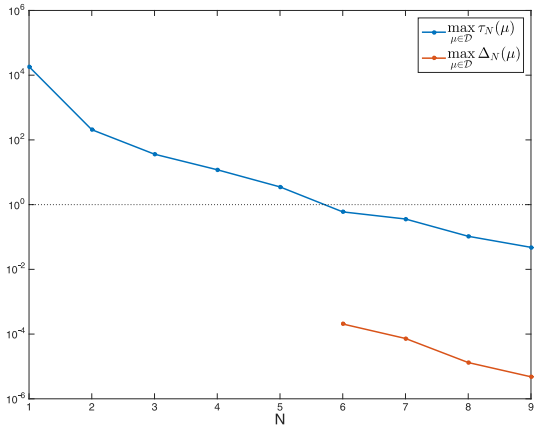

Figure 7 Convergence of the Greedy algorithm

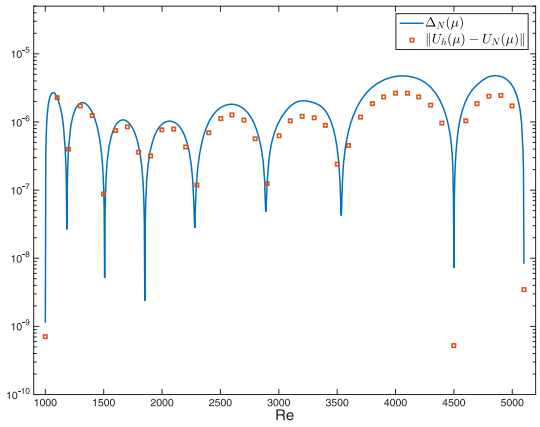

Figure 8 Value of $\Delta_{N_{\max}}(\mu)$ and the error between the FE solution and the RB solution

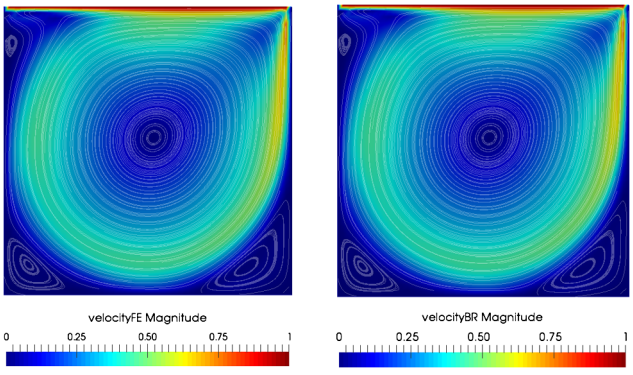

Figure 9 FE solution (left) and RB solution (right) for $\mu = 2142$

Table 2 Computational time for FE solution and RB online phase, with the speed-up and the relative error

Data	$\mu = 1620$	$\mu = 2142$	$\mu = 3693$	$\mu = 4745$
T_{FE}	1486.4 s	1972.1 s	3089.3 s	3777.51 s
T_{online}	0.51 s	0.52 s	0.52 s	0.52 s
speed-up	2869	3773	5935	7264
$\|\mathbf{u}_h - \mathbf{u}_N\|_{\mathbf{x}_h}$	$1.9 \cdot 10^{-6}$	$1.58 \cdot 10^{-6}$	$2.62 \cdot 10^{-6}$	$4.99 \cdot 10^{-6}$
$\|p_h - p_N\|_{\mathbb{M}_h}$	$2.94 \cdot 10^{-7}$	$1.79 \cdot 10^{-7}$	$1.11 \cdot 10^{-7}$	$1.25 \cdot 10^{-7}$

sky solution, and the online phase computational time of the RB model in both cases are similar.

6 Conclusions

The numerical studies performed in the present paper indicate that the considered LPS method is able to reproduce first and second-order statistics up to a turbulent regime for relatively coarse meshes, with a similar (or even higher) accuracy than a more complex VMS-LES method [26]. We studied the parallel performances of the proposed solver implemented in a HPC framework, showing rather good scalability results up to thousands

of cores. This promotes the present method as a suitable and useful tool in the challenging simulation of turbulent flows, since providing reliable numerical results with a comparatively small computational complexity, which is an extremely important feature in the context of realistic industrial applications in CFD. We also presented a RB VMS-Smagorinsky model, for which we developed an *a posteriori* error bound estimator, and we presented a numerical test in which we showed a speed-up of several thousands in the computation of the numerical solution of the VMS-Smagorinsky model. We thus enhanced the results presented in [30], considering a more accurate high-order method, with higher speed-up in the computation of the RB solution in the online phase.

Acknowledgements
The research of the authors has been partially supported by the Spanish Government Project MTM2015-64577-C2-1-R.

Funding
The research of the authors has been partially supported by the Spanish Government Project MTM2015-64577-C2-1-R.

Abbreviations
LES, Large eddy simulation; NSE, Navier–Stokes equations; FE, Finite element; LPS, Local projection stabilization; RB, Reduced basis; BDF, Backward differentiation formula; IBVP, Initial boundary value problem; VMS, Variational multi-scale; DDM, Domain decomposition method; HPC, High performance computing; DNS, Direct numerical simulation; CFD, Computational fluid dynamics; TGL, Taylor–Görtler-like; BRR, Brezzi–Rappaz–Raviart.

Availability of data and materials
Data sharing not applicable to this article as no datasets were generated or analysed during the current study.

Competing interests
The authors declare that they have no competing interests.

Authors' contributions
All authors contributes to this paper as a whole. All authors read and approved the final manuscript.

Authors' information
Not applicable.

Publisher's Note

Received: 15 March 2018 Accepted: 29 May 2018 Published online: 08 June 2018

References

1. Chacón Rebollo T, Gómez Mármol M, Girault V, Sánchez Muñoz I. A high order term-by-term stabilization solver for incompressible flow problems. IMA J Numer Anal. 2013;33(3):974–1007. https://doi.org/10.1093/imanum/drs023.
2. Braack M, Burman E. Local projection stabilization for the Oseen problem and its interpretation as a variational multiscale method. SIAM J Numer Anal. 2006;43(6):2544–66.
3. Knobloch P, Lube G. Local projection stabilization for advection–diffusion–reaction problems: one-level vs. two-level approach. Appl Numer Math. 2009;59(12):2891–907. https://doi.org/10.1016/j.apnum.2009.06.004.
4. Chacón Rebollo T. A term by term stabilization algorithm for finite element solution of incompressible flow problems. Numer Math. 1998;79(2):283–319. https://doi.org/10.1007/s002110050341.
5. Ahmed N, Chacón Rebollo T, John V, Rubino S. Analysis of a full space-time discretization of the Navier–Stokes equations by a local projection stabilization method. IMA J Numer Anal. 2017;37(3):1437–67. https://doi.org/10.1093/imanum/drw048.
6. Chacón Rebollo T, Gómez Mármol M, Restelli M. Numerical analysis of penalty stabilized finite element discretizations of evolution Navier–Stokes equation. J Sci Comput. 2015;63(3):885–912.
7. Haferssas R, Jolivet P, Rubino S. Efficient and scalable discretization of the Navier–Stokes equations with LPS modeling. Comput Methods Appl Mech Eng. 2018;333:371–94. https://doi.org/10.1016/j.cma.2018.01.026.
8. Chacón Rebollo T, Lewandowski R. Mathematical and numerical foundations of turbulence models and applications. Basel: Birkhäuser; 2014.
9. Codina R. Comparison of some finite element methods for solving the diffusion–convection–reaction equation. Comput Methods Appl Mech Eng. 1998;156(1–4):185–210. https://doi.org/10.1016/S0045-7825(97)00206-5.
10. Scott RL, Zhang S. Finite element interpolation of non-smooth functions satisfying boundary conditions. Math Comput. 1990;54(190):483–93.
11. Hecht F. New development in freefem++. J Numer Math. 2012;20(3–4):251–65.
12. Badia S. On stabilized finite element methods based on the Scott–Zhang projector. Circumventing the inf-sup condition for the Stokes problem. Comput Methods Appl Mech Eng. 2012;247/248:65–72.

13. Ahmed N, Chacón Rebollo T, John V, Rubino S. A review of variational multiscale methods for the simulation of turbulent incompressible flows. Arch Comput Methods Eng. 2017;24(1):115–64. https://doi.org/10.1007/s11831-015-9161-0.
14. Chacón Rebollo T, Gómez Mármol M, Rubino S. Finite element approximation of an unsteady projection-based VMS turbulence model with wall laws. In: Boundary and interior layers, computational and asymptotic methods—BAIL 2014. Lect. notes comput. sci. eng. vol. 108. Berlin: Springer; 2015. p. 47–73.
15. Chacón Rebollo T, Gómez Mármol M, Rubino S. Numerical analysis of a finite element projection-based VMS turbulence model with wall laws. Comput Methods Appl Mech Eng. 2015;285:379–405. https://doi.org/10.1016/j.cma.2014.11.023.
16. Chacón Rebollo T, Hecht F, Gómez Mármol M, Orzetti G, Rubino S. Numerical approximation of the Smagorinsky turbulence model applied to the primitive equations of the ocean. Math Comput Simul. 2014;99:54–70. https://doi.org/10.1016/j.matcom.2013.04.023.
17. Chacón Rebollo T, Gómez Mármol M, Hecht F, Rubino S, Sánchez Muñoz I. A high-order local projection stabilization method for natural convection problems. J Sci Comput. 2018;74(2):667–92. https://doi.org/10.1007/s10915-017-0469-9.
18. Rubino S. Numerical modeling of turbulence by richardson number-based and VMS models. PhD thesis. University of Seville; 2014.
19. Codina R. A stabilized finite element method for generalized stationary incompressible flows. Comput Methods Appl Mech Eng. 2001;190(20–21):2681–706. https://doi.org/10.1016/S0045-7825(00)00260-7.
20. Dolean V, Jolivet P, Nataf F. An introduction to domain decomposition methods: algorithms, theory, and parallel implementation. Philadelphia: SIAM; 2015.
21. Jolivet P, Hecht F, Nataf F, Prud'homme C. Scalable domain decomposition preconditioners for heterogeneous elliptic problems. In: Proceedings of the 2013 ACM/IEEE conference on supercomputing; 2013.
22. Haferssas R, Jolivet P, Nataf F. An additive Schwarz method type theory for Lions's algorithm and a symmetrized optimized restricted additive Schwarz method. SIAM J Sci Comput. 2017;39(4):1345–65.
23. Gravemeier V. Scale-separating operators for variational multiscale large eddy simulation of turbulent flows. J Comput Phys. 2006;212(2):400–35. https://doi.org/10.1016/j.jcp.2005.07.007.
24. Moser R, Kim J, Mansour NN. Direct numerical simulation of turbulent channel flow up to $Re_\tau = 590$. Phys Fluids. 1999;11(4):943–5.
25. John V, Kindl A. Numerical studies of finite element variational multiscale methods for turbulent flow simulations. Comput Methods Appl Mech Eng. 2010;199(13–16):841–52. https://doi.org/10.1016/j.cma.2009.01.010.
26. Gravemeier V, Wall WA, Ramm E. Large eddy simulation of turbulent incompressible flows by a three-level finite element method. Int J Numer Methods Fluids. 2005;48(10):1067–99. https://doi.org/10.1002/fld.961.
27. Prasad AK, Koseff JR. Reynolds number and end-wall effects on a lid-driven cavity flow. Phys Fluids. 1989;1:208–18.
28. Forti D, Dedè L. Semi-implicit BDF time discretization of the Navier–Stokes equations with VMS–LES modeling in a high performance computing framework. Comput Fluids. 2015;117:168–82. https://doi.org/10.1016/j.compfluid.2015.05.011.
29. Chacón Rebollo T, Delgado Ávila E, Gómez Mármol M, Rubino S. A self-adapting LPS solver for laminar and turbulent fluids in industry and hydrodynamic flows. In: Progress in industrial mathematics at ECMI 2016. Mathematics in industry. vol. 26. Berlin: Springer; 2017. p. 561–8.
30. Chacón Rebollo T, Delgado Ávila E, Gómez Mármol M, Ballarin F, Rozza G. On a certified Smagorinsky reduced basis turbulence model. SIAM J Numer Anal. 2017;55(6):3047–67. https://doi.org/10.1137/17M1118233.
31. Bernardi C, Maday Y, Rapetti F. Discrétisations variationnelles de problèmes aux limites elliptiques. Mathématiques & applications. vol. 45. Berlin: Springer; 2004. p. 310.
32. Grelp MA, Maday Y, Nguyen NC, Patera AT. Efficient reduced-basis treatment of nonaffine and nonlinear partial differential equations. ESAIM: Math Model Numer Anal. 2007;41(3):575–605.
33. Manzoni A. An efficient computational framework for reduced basis approximation and a posteriori error estimation of parametrized Navier–Stokes flows. ESAIM: Math Model Numer Anal. 2014;48:1199–226.
34. Brezzi F, Rappaz J, Raviart PA. Finite dimensional approximation of nonlinear problems. Numer Math. 1980;36:1–25.
35. Caloz G, Rappaz J. Numerical analysis for nonlinear and bifurcation problems. In: Handbook of numerical analysis. vol. V; 1997.